Electrically pumped InP-based microdisk lasers integrated with a nanophotonic silicon-on-insulator waveguide circuit

J. Van Campenhout[1], P. Rojo-Romeo[2], P. Regreny[2], C. Seassal[2], D. Van Thourhout[1], S. Verstuyft[1], L. Di Cioccio[3], J.-M. Fedeli[3], C. Lagahe[4] and R. Baets[1]

[1]*Ghent University-IMEC, Photonics Research Group, Sint-Pietersnieuwstraat 41, 9000 Ghent, Belgium*
[2] *Institut des Nanotechnologies de Lyon, Ecole Centrale de Lyon, 36 Avenue Guy de Collongue, 69134 Ecully, France*
[3]*CEA-DRT/LETI, 17 Rue des Martyrs, 38054 Grenoble cedex 9 - France.*
[4]*TRACIT Technologies, Zone Astec - 15, rue des Martyrs, 38054 Grenoble, France*
joris.vancampenhout@intec.ugent.be

Abstract: A compact, electrically driven light source integrated on silicon is a key component for large-scale integration of electronic and photonic integrated circuits. Here we demonstrate electrically injected continuous-wave lasing in InP-based microdisk lasers coupled to a sub-micron silicon wire waveguide, fabricated through heterogeneous integration of InP on silicon-on-insulator (SOI). The InP-based microdisk has a diameter of 7.5 μm and a thickness of 1 μm. A tunnel junction was incorporated to efficiently contact the p-side of the pn-junction. The laser emits at 1.6 μm, with a threshold current as low as 0.5 mA under continuous-wave operation at room temperature, and a threshold voltage of 1.65 V. The SOI-coupled laser slope efficiency was estimated to be 30 μW/mA, with a maximum unidirectional output power of 10 μW.

©2007 Optical Society of America

OCIS codes: (140.5960) Semiconductor lasers; (250.5300) Photonic integrated circuits

References and links

1. W. Bogaerts, R. Baets, P. Dumon, V. Wiaux, S. Beckx, D. Taillaert, B. Luyssaert, J. Van Campenhout, P. Bienstman, D. Van Thourhout, "Nanophotonic waveguides in silicon-on-insulator fabricated with CMOS technology," IEEE J. of Lightwave Technol. **23**, 401-412, (2005).
2. R. Soref, "The past, present and future of silicon photonics," IEEE J. Sel. Tops. Quantum Electron. **12**, 1687-1687 (2006).
3. H. S. Rong, R. Jones, A. S. Liu, O. Cohen, D. Hak, A. Fang, M. J. Paniccia, "A continuous-wave Raman silicon laser," Nature **433**, 725-728 (2005).
4. O. Boyraz and B. Jalali, "Demonstration of a silicon Raman laser," Opt. Express **12**, 5269 (2004).
5. L. Pavesi, L. Dal Negro, C. Mazzoleni, G. Franzò, and F. Priolo, "Optical gain in silicon nanocrystals," Nature **408**, 440–444 (2000).
6. S. Lombardo, S. Campisano, G. Vandenhoven, A. Cacciato, and A. Polman "A Room-temperature Luminescence from Er3+-implanted semi-insulating polycrystalline silicon," Appl. Phys. Lett. **63**, 1942–1944 (1993).
7. G. Roelkens, D. Van Thourhout, R. Baets, R. Notzel, and M. Smit, "Laser emission and photodetection in an InP/InGaAsP layer integrated on and coupled to a silicon-on-insulator waveguide circuit," Opt. Express **14**, 8154-8159 (2006).
8. A. W. Fang, H. Park, O. Cohen, R. Jones, M. J. Paniccia, J. E. Bowers, "Electrically pumped hybrid AlGaInAs-silicon evanescent laser," Opt. Express **14**, 9203-9210 (2006).
9. A. W. Fang, R. Jones, H. Park, O. Cohen, O. Raday, M. J. Paniccia, J. E. Bowers, "Integrated AlGaInAs-silicon evanescent racetrack laser and photodetector," Opt. Express **14**, 9203-9210 (2006).
10. D. A. B. Miller, "Optical interconnects to silicon," IEEE J. Sel. Top. Quantum Electron. **6**, 1312−1317 (2000).
11. T. Baba, M. Fujita, A. Sakai, M. Kihara, R. Watanabe, "Lasing characteristics of GaInAsP-InP strained quantum-well microdisk injection lasers with diameter of 2-10μm," IEEE Photon. Technol. Lett. **9**, 878-880 (1997).
12. C. J. Seung, K. Djordjev, S. J. Choi, and P. D. Dapkus," Microdisk lasers coupled to output waveguides," IEEE Photon. Technol. Lett. **15**, 1330-1332 (2003).

#81363 - $15.00 USD Received 22 Mar 2007; revised 27 Apr 2007; accepted 27 Apr 2007; published 17 May 2007

13. P. Rojo Romeo, J. Van Campenhout, P. Regreny, A. Kazmierczak, C. Seassal, X. Letartre, G. Hollinger, D. Van Thourhout, R. Baets, J. M. Fedeli, and L. Di Cioccio, "Heterogeneous integration of electrically driven microdisk based laser sources for optical interconnects and photonic ICs," Opt Express **14**, 3864-3871 (2006).
14. J. Van Campenhout, P. Rojo Romeo, D. Van Thourhout, C. Seassal, P. Regreny, L. Di Cioccio, J. M. Fedeli, and R. Baets, "Thermal characterisation of electrically injected thin-film InGaAsP microdisk lasers on Si," IEEE J. Lightwave Technol. (to be published).
15. H. T. Hattori, C. Seassal, E. Touraille, P. Rojo Romeo, X. Letartre, G. Hollinger, P. Viktorovitch, L. Di Cioccio, M. Zussy, L. El Melhaoui, and J. M. Fedeli, "Heterogeneous integration of microdisk lasers on silicon strip waveguides for optical interconnects," IEEE Photon. Technol. Lett. **18**, 223-225 (2006).
16. M. T. Hill, H. J. S. Dorren, T. De Vries, X. J. M. Leijtens, J. H. den Besten, B. Smalbrugge, Y. S. Oei, H. Binsma, G. D. Khoe, and M. K. Smit, "A fast low-power optical memory based on coupled micro-ring lasers," Nature **432**, 206-209 (2004).
17. M. T. Hill, E. Frietman, H. de Waardt, G. Khoe, and H. J. S. Dorren, "All fiber-optic neural network using coupled SOA based ring lasers," IEEE Trans. Neural Networks **13**, 1504-1513 (2002).
18. J. Boucart, C. Starck, F Gaborit, A. Plais, N. Bouche, E. Derouin, J. C. Remy, J. Bonnet-Gamard, L. Goldstein, C. Fortin, D. Carpentier, P. Salet, F. Brillouet, J. Jacquet, "Metamorphic DBR and Tunnel-Junction Injection: A CW RT Monolithic Long-Wavelength VCSEL", IEEE J. Sel. Tops. Quantum Electron **5**, 520-529 (1999).
19. M. Kostrzewa, L. Di Cioccio, M. Zussy, J. C. Roussin, J. M. Fedeli, N. Kernevez, P. Regreny, C. Lagahe-Blanchard, B. Aspar, "InP dies transferred onto silicon substrate for optical interconnects application," Sensors and Actuators A: Physical **125**, 411-414 (2006).
20. D. Taillaert, F. Van Laere, M. Ayre, W. Bogaerts, D. Van Thourhout, P. Bienstman, R. Baets, "Grating couplers for coupling between optical fibers and nanophotonic waveguides," Jpn. J. Appl. Phys. **45**, 6071-6077 (2006).
21. M. Sorel, G. Giuliani, A. Scire, R. Miglierina, S. Donati, P. J. R. Laybourn, "Operating regimes of GaAs–AlGaAs semiconductor ring lasers: experiment and model," IEEE J. Quantum Electron. **39**, 1187-1195 (2003).
22. B. E. Little, J.-P Laine and S. T. Chu, "Surface-roughness-induced contradirectional coupling in ring and disk resonators," Opt Lett. **22**, 4-6 (1997).
23. I. Christiaens, "Vertically coupled microring resonators fabricated with wafer bonding," PhD thesis, Ghent University, 2005.

1. Introduction

In recent years, silicon-on-insulator (SOI) has emerged as a promising platform for passive photonic functions due to the transparency of silicon at telecom wavelengths, its high refractive index contrast and the fact that complementary metal oxide semiconductor (CMOS) technology can be used for fabricating photonic devices with sub-micron features [1,2]. However, a major obstacle for large-scale silicon-based electronic-photonic integration is the absence of a compact and efficient silicon-based light source, due to the indirect band gap of silicon. Various strategies for light emission in silicon have been demonstrated [3-6]. However, compact and efficient active devices don't seem feasible in the short term. Efficient active photonic functionality can be added to the SOI platform by bonding a thin film of direct band gap material such as InP on top of it. Lasers and detectors can be fabricated in this thin film and can be coupled to the SOI waveguide circuit [7-9]. Some applications however, such as on-chip optical interconnect [10], can strongly benefit from dense electronic-photonic integration. Hence, the laser footprint and power consumption should be made very small. The approach presented in Ref. [7] uses long, adiabatic tapers to couple the laser output into the SOI waveguide, which are not compatible with small device footprint. For the hybrid architecture used in Ref.s [8, 9], optical confinement is provided only by the SOI platform. While this approach relaxes the alignment tolerances, it seems difficult to fabricate ultracompact laser cavities with low optical loss combined with sufficient confinement in the InP-based gain region. Therefore, our work focuses on the heterogeneous integration of ultra-compact InP-based microdisk lasers [11-12] on the silicon platform. In this case, optical confinement is primarily in the InP layer with evanescent coupling to the SOI waveguide, allowing micron-sized laser cavities. With the bonding approach, CMOS technology could be used to fabricate and integrate thousands of low-power microlasers on a single die.

#81363 - $15.00 USD Received 22 Mar 2007; revised 27 Apr 2007; accepted 27 Apr 2007; published 17 May 2007
(C) 2007 OSA

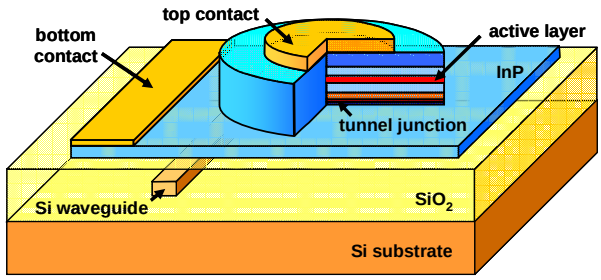

Fig. 1. Schematic drawing of the heterogeneous microdisk laser structure, showing the disk cavity, SOI wire waveguide, bottom contact layer, tunnel junction and metal contacts.

Table 1. Epitaxial layer composition

Layer description	Material	Doping (cm^{-3})	Thickness (nm)
Top contact	n-type InP	$5x10^{18}$	340
Confinement layer	n-type Q1.2	$1x10^{18}$	100
Barrier	Q1.2	undoped	20 (3x)
Quantum well	InAsP	undoped	6 (3x)
Confinement layer	Q1.2	undoped	100
p-side junction	p-type InP	$1x10^{18}$	220
Tunnel junction	p-type Q1.2	$2x10^{19}$	20
Tunnel junction	n-type Q1.2	$2x10^{19}$	20
Bottom lateral contact	n-type InP	$5x10^{18}$	100

Previously we demonstrated electrically injected lasing in microdisk structures integrated on a plain silicon wafer, with threshold currents as low as 550 μA [13, 14]. Only pulsed operation was achieved due to the high thermal resistance in combination with a large electrical resistance. The coupling to an SOI wire waveguide was also demonstrated for an optically pumped microdisk laser [15]. In this paper, we report on the integration of an electrically injected microdisk laser on the SOI waveguide platform. Continuous-wave operation at room-temperature was obtained by reducing the operating voltage and substantial coupling into the SOI waveguide was achieved by reducing the bonding layer thickness. We believe that this device has great potential for on-chip interconnect, but can also enable more advanced functionality such as compact optical memories [16] and on-chip optical neural networks [17] by coupling different microdisk lasers.

2. Microdisk laser structure and fabrication

A schematic representation of the laser structure is given in Fig. 1. A microdisk is etched in a thin InP-based layer bonded on top of a SOI waveguide wafer. The fundamental optical resonances in such a structure are *whispering-gallery* modes (WGM), which are confined to the edges of the microdisk. Therefore, a top metal contact can be placed in the centre of the microdisk, without adding extra optical losses. The bottom contact is positioned on a thin lateral contact layer: this layer will cause no substantial additional optical losses, provided it is sufficiently thin. Another issue in the design of electrically injected thin-film microlasers is how to make a p-type contact with low contact resistance. In a classic substrate laser, this is done by using heavily doped, low-bandgap contact layers. This cannot be done for a thin-film

#81363 - $15.00 USD Received 22 Mar 2007; revised 27 Apr 2007; accepted 27 Apr 2007; published 17 May 2007
(C) 2007 OSA

laser structure, as this would cause excessive internal absorption losses. Therefore, we

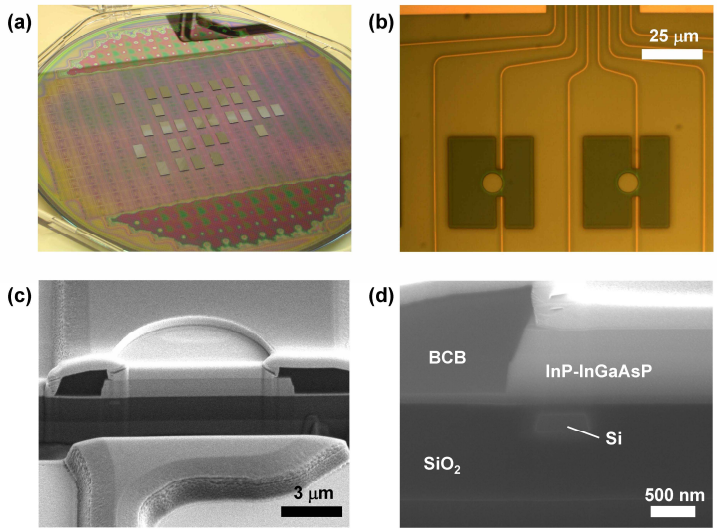

Fig. 2. 200-mm SOI-wafer with bonded InP dies (a), top view of two InP islands with microdisk lasers before metallization and visible SOI waveguides (b), focused-ion-beam cross-section of the microdisk (c), detail of the disk edge, also showing the SOI wire waveguide (d).

implemented a tunnel junction with low optical loss [18] in combination with another n-type contact, instead of low-bandgap p-type contact layer. The laser resonance is evanescently coupled to the underlying SOI waveguide, which is vertically aligned with the edge of microdisk.

First, a 200 mm silicon-on-insulator waveguide wafer was fabricated using CMOS processes as described in Ref. [1]. The wire waveguides have a width of 550 nm and a height of 220 nm. The buried oxide layer thickness is 1 μm. Next, a 750-nm thick TEOS-SiO_2 layer was deposited. E-beam alignment features were then etched down to the buried oxide layer. The SOI-wafer was then planarized by chemical-mechanical polishing (CMP), until approximately 125 nm SiO_2 was left on top of the SOI waveguides. An InP-based epilayer structure was grown by Molecular Beam Epitaxy on a two-inch InP wafer. The active layer structure consists of three compressively strained InAsP quantum wells (6 nm), in unstrained Q1.2 barrier layers (20 nm). The heterostructure contains n-type contact layers ($5x10^{18}$ cm^{-3}), and a tunnel junction consisting of a 20-nm heavily doped p-type layer ($2x10^{19}cm^{-3}$) and a 20-nm heavily doped n-type layer ($1x10^{19}$ cm^{-3}). An overview of the laser structure can be found in Table 1. A 300 nm sacrificial InGaAs etch-stop layer was also included, for substrate removal. After MBE-growth, a thin 10 nm SiO_2 layer was deposited by Electron Cyclotron Resonance (ECR). Then, the III-V wafer was diced into pieces with a dimension of 9x5 mm^2. These dies were then molecularly bonded to the SOI waveguide wafer [19], with only a coarse alignment. Finally, the InP substrate and the InGaAs etch stop layer of the dies were removed by HCl and $FeCl_3$ solutions. On this SOI wafer with bonded laser dies, a 150-nm thick SiO_2 hard mask was deposited. The microdisk structures were defined by e-beam lithography, aligned to the SOI waveguides using the e-beam alignment features, and transferred to the hard mask. After this step, the SOI wafer was diced and the further processing was done on individual dies. However, in principle, wafer scale technology could be used. First, the microdisk cavities were partially etched by reactive ion etching, leaving a thin bottom contact layer of about 100 nm. The etching depth was carefully controlled by in-situ laser interferometry,since too

#81363 - $15.00 USD Received 22 Mar 2007; revised 27 Apr 2007; accepted 27 Apr 2007; published 17 May 2007
(C) 2007 OSA

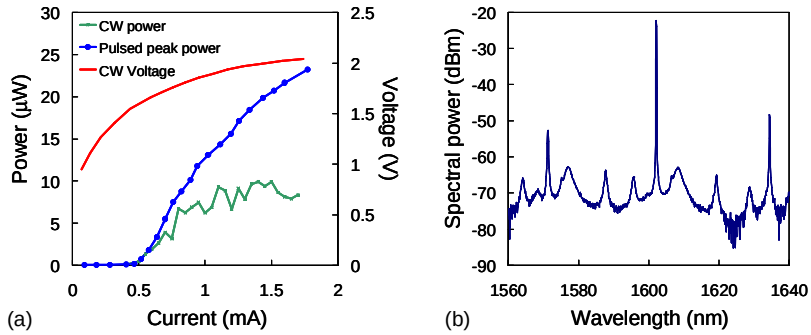

Fig. 3. Lasing characteristics at 20 °C for a 7.5-µm disk (a). Continuous-wave lasing spectrum for 1.4 mA, normalized for the fiber-coupler efficiency and on-chip propagation loss (b).

thick contact layers cause excessive bend loss, whereas too thin contact layer increases the electrical resistance of the device. Then, the bottom contact layer was removed where it isn't needed. A 1.5-µm thick benzocyclobutene (BCB) layer was then spun on top of the laser structures. In this BCB layer, contact windows were etched, both for the bottom contact and the top contact. The opening of the top contact window requires additional attention, since its shape defines where the top metal is in contact with the laser cavity: a too big window causes optical absorption at the metal, whereas a too small window can cause inefficient current injection. Finally, Ti/Pt/Au metal layers were deposited and subjected to a rapid thermal anneal at 325 °C to form the bottom and top contacts. Images during various stages of the fabrication are shown in Fig. 2.

3. Measurement results and discussion

The microdisk lasers were activated by applying a positive voltage to the bottom contact. The output power was collected at one end of the output SOI waveguide, using a fiber grating coupler [20]. For microdisk lasers with 7.5-µm diameter, we observed continuous-wave lasing at room temperature (20 °C). Figure 3(a) shows the output power and the device voltage versus the input current. The threshold current is 0.5 mA, which is equivalent with 1.13 kA/cm^2, assuming uniform injection. The threshold voltage is about 1.65 V. The output spectrum for 1.4 mA - normalized for the fiber coupler spectrum - is shown in Fig. 3(b). It reveals three fundamental WGMs, separated by a free spectral range of 32 nm, which is equivalent with a group index of 3.4. The WGM at 1.6 µm is lasing with a laser linewidth that is smaller than the resolution limit of the measurement setup (60 pm). The slope efficiency just above threshold was estimated to be 30 µW/mA, assuming a fiber coupler efficiency of 25 % at the lasing wavelength and 2 dB on-chip propagation losses. The maximum continuous-wave output power is 10 µW. In pulsed operation, output peak powers up to 100 µW have been measured. The early thermal roll-over in continuous-wave regime is caused by a high thermal resistance, which was measured to be 10 K/mW, in agreement with simulation [14]. The abrupt kinks in the continuous-wave L-I curve for currents larger than 0.75 mA are most likely due to mode competition between the clockwise and counter-clockwise laser mode, which is a typical behaviour for ring lasers [21]. For an ideal microdisk, these counterpropagating modes are degenerate. However, the presence of surface roughness induces contradirectional coupling between the two modes, lifting the degeneracy and causing mode splitting [22]. While our device exhibits substantial sidewall roughness, the lasing spectra didn't show any evidence of such mode splitting, suggesting it is much smaller than the resolution limit of 60 pm, or that lasing occurs in only one of the laser modes for a given pumping level. Monitoring the laser output at both SOI waveguide ends should bring more insight in this mode competition, but was not possible on the available samples. The sample contained microdisk lasers with variable top metal contact sizes (5.3-6.3 µm). It

#81363 - $15.00 USD Received 22 Mar 2007; revised 27 Apr 2007; accepted 27 Apr 2007; published 17 May 2007
(C) 2007 OSA

was found that laser performance depends strongly on the position and size of the top metal. The top contact was misaligned by about 400 nm during lithography, as can be seen in Fig. 2(c). As a result, only the lasers with smallest top contact showed low-threshold continuous-wave lasing. For bigger top contacts, laser performance was worse due to absorption loss at the misaligned top metal.

For the microdisk laser with fabricated dimensions, the bend loss is calculated to be negligible, the internal loss to be 11 cm^{-1} and the distributed coupling loss to be 9.5 cm^{-1}, all with respect to the disk circumference. This is equivalent with an extraction efficiency of 46 %. While the top metal is only applied to the center of the microdisk, uniform injection is expected due to current spreading in the highly conductive top n-type contact layer. Considering the fact that the WGM has a radial width of about 20 % of the disk radius at the edge of the disk, the lateral injection efficiency is approximately 36 %. Assuming a vertical injection efficiency of 0.7, and accounting for two degenerate, counterpropagating laser modes, results in a theoretical unidirectional slope efficiency of 46 μW/mA. The measured slope efficiency of 30 μW/mA is lower than the theoretical efficiency, most likely due to scattering loss at the disk edge. Agreement between simulation and measurement can be obtained by assuming a scattering loss of 10 cm^{-1}. While this value is relatively high, it agrees with scattering losses extracted for passive, InP-based ring resonators, fabricated in our group [23]. Simulations indicate that the coupling loss is very sensitive to the bonding layer thickness and the wire waveguide width. Also, a Secondary Ion Mass Spectroscopy analysis on test samples indicates that the true tunnel-junction doping level is $8x10^{18}$ cm^{-3} rather than is $2x10^{19}$ cm^{-3}. Hence, we might slightly overestimate the internal absorption loss. For the above reasons, the match between theory and experiment is qualitative rather than quantitative.

Nevertheless, higher efficiencies could be obtained by reducing the sidewall roughness while improving the coupling efficiency, for instance by reducing the bonding layer thickness or by using curved SOI waveguides. Further performance improvement could be possible by improving the lateral injection efficiency, for instance by etching a hole in the center of the disk. Increasing the lateral injection efficiency by a factor two seems feasible, thereby reducing the threshold and improving the slope efficiency with the same factor. Finally, the thermal resistance could be reduced by incorporating a thermal via that provides a thermally conductive connection between the top contact and the Si substrate. A combination of the above strategies should bring a threshold current of 250 μA with a slope efficiency of 100 μW/mA within reach.

4. Conclusion

We have demonstrated electrically-injected continuous-wave lasing at room temperature in microdisk lasers integrated on and coupled to a nanophotonic silicon-on-insulator waveguide circuit. The microdisks were fabricated in a thin InP-based film, which was directly bonded to the waveguide SOI wafer. CMOS technology can be used for fabrication on wafer scale. The threshold current was 0.5 mA, and the unidirectional slope efficiency was 30 μW/mA, with a maximum continuous-wave output power of 10 μW. The output power and efficiency can be greatly enhanced by reducing sidewall scattering loss and by improving the lateral injection efficiency and the optical coupling between the InP disk and the Si waveguide. We conclude that this device has great potential for dense and cost-effective electronic-photonic integration.

Acknowledgments

The authors would like to thank Jan Van den Troost and Liesbet Van Landschoot for part of the III-V processing. Part of this work was performed in the framework of the EU-funded FP6-project PICMOS and the FP6 network-of-excellence ePIXnet. J. Van Campenhout was supported by the Research Foundation – Flanders (FWO-Vlaanderen) through a doctoral fellowship.

#81363 - $15.00 USD Received 22 Mar 2007; revised 27 Apr 2007; accepted 27 Apr 2007; published 17 May 2007
(C) 2007 OSA